

Full length article

Squared and rectangular QAM compatible decoder for spectrally efficient frequency division multiplexing optical systems

Peiji Song^a, Zhouyi Hu^{b,*}, Hongyao Chen^{a,c}, Chun-Kit Chan^a^a Department of Information Engineering, The Chinese University of Hong Kong, Hong Kong, China^b Department of Electrical Engineering, Eindhoven University of Technology, 5600 MB Eindhoven, The Netherlands^c School of Computer and Communication Engineering, University of Science and Technology Beijing, Beijing 100091, China

ABSTRACT

We propose a squared and rectangular quadrature amplitude modulation (QAM) compatible decoder (SRCD) for spectrally efficient frequency division multiplexing (SEFDM) systems, which can be applied to M^2 ($M = 2^p$, $p = 1, 2, 3, \dots$) QAM and rectangular QAM constellations without needing specifically designed soft mapping strategies, showing better transmission performance compared to the conventional iterative detection (ID) decoder. Different from the ID decoder, the proposed SRCD applies separate detection to the in-phase and the quadrature components of complex-valued symbols based on the real-valued property of the correlation matrix, leading to better performance. To verify the effectiveness of the proposed scheme, we experimentally study the performance of four different types (circular, rectangular, star, and square constellations) of 8-QAM using SRCD or ID in SEFDM systems. Experimental results have shown that the rectangular 8-QAM with SRCD can achieve a spectral gain of about 11.1 %, while still outperforming other 8-QAM formats without bandwidth compression, indicating the superiority of the proposed SRCD in SEFDM optical systems.

1. Introduction

Given the advantages such as high cost-effectiveness and simple implementation, the intensity-modulation/direct-detection (IM/DD) optical system has been extensively studied in some important scenarios such as data center networks, visible light communications, and passive optical networks [1–3]. Different from coherent optical systems [4], only the dimension of intensity is utilized to carry signals in IM/DD optical systems. Therefore, low spectral efficiency (SE) becomes one of their primary disadvantages. To cope with this challenge, many advanced modulation formats have been investigated for IM/DD optical systems, e.g., pulse amplitude modulation (PAM), carrier-less amplitude and phase modulation (CAP), half-cycle quadrature amplitude modulation (QAM), and orthogonal frequency-division multiplexing (OFDM) [5–8], among which OFDM possesses the merits of flexible modulation and robustness against fiber chromatic dispersion (CD) [9].

Recently, by further reducing frequency spacing between neighboring subcarriers beyond the Nyquist limit, spectrally efficient frequency division multiplexing (SEFDM) was proposed and has received extensive attention in the fields of wireless and optical communications due to its higher SE than OFDM can hold [10,11]. However, the purposely induced violation of the orthogonality results in additional inter-carrier interference (ICI) which becomes the prominent impairment in

SEFDM systems [12–14]. To effectively eliminate ICI, maximum likelihood (ML) was proposed as the optimum detector. However, its exponential computational complexity prevents it from being implemented in practical applications [15,16]. In [17], to realize ML detection with reduced complexity, the authors proposed employing a sphere decoder (SD) whose complexity still increases significantly when the SEFDM system has a large number of subcarriers, small bandwidth compression factor (BCF), or low signal-to-noise ratio (SNR) level [14]. On the other hand, some linear algorithms such as zero-forcing (ZF) and minimum mean squared error (MMSE) have proven to be no longer feasible for SEFDM due to the influence of ICI [18–21]. Therefore, to realize efficient detection with relatively low complexity in SEFDM systems, iterative detection (ID) with soft decision was proposed in [22]. However, the ID algorithm needs different mapping strategies for different modulation formats modulated onto the subcarriers of SEFDM signals, which can be attributed to its joint detection of the in-phase and quadrature (I/Q) components of complex-valued symbols, leading to limited transmission performance [23]. The cascaded binary-phase-shift-keying iterative detection (CBID) was proposed in [24] to solve the constraints of ID. However, it is still limited to the application of squared QAM constellations due to its joint iteration of the I and Q components. For non-squared QAM constellations, such as rectangular 8-QAM constellations and 32-QAM constellations, the decoding still needs to be implemented

* Corresponding author.

E-mail address: z.hu@tue.nl (Z. Hu).<https://doi.org/10.1016/j.optlastec.2023.109776>

Received 29 December 2022; Received in revised form 11 June 2023; Accepted 25 June 2023

Available online 30 June 2023

0030-3992/© 2023 The Authors. Published by Elsevier Ltd. This is an open access article under the CC BY license (<http://creativecommons.org/licenses/by/4.0/>).

by the conventional ID algorithm with specifically designed mapping strategies [25].

In this work, based on the real-valued property of the correlation matrix of the SEFDM system, we propose a squared and rectangular QAM compatible decoder (SRCD). The proposed SRCD can separately detect the I/Q components of complex-valued symbols by iterating the I/Q components separately, which is different from the joint iteration of the I/Q components in CBID, and is, therefore, suitable for both squared (e.g., M^2 -QAM, where $M = 2^p$, $p = 1, 2, 3, \dots$) and rectangular QAM constellations. By using this SRCD, we can achieve better decoding performance in eliminating ICI than the conventional ID algorithm can, and at the same time solve the limitation of CBID that can only be applied to squared QAM constellations, thus improving compatibility and flexibility. We further investigate the performance of four different 8-QAM formats, i.e., circular, rectangular, star, and square constellations, used in SEFDM systems. Experimental results show that the conventional ID is sensitive to different 8-QAM formats by comparing it in an SEFDM system with the logarithmic-maximum-a-posteriori (log-MAP) Viterbi decoder [14] that is a maximum likelihood demodulation algorithm and the conventional OFDM system without bandwidth compression. When the ID or the SRCD is used, the rectangular 8-QAM format with the proposed SRCD can outperform the other schemes. Specifically, under a bandwidth-limited scenario, the experimental results show that the proposed scheme can achieve a spectral gain of about 11.1 %, while still outperforming the other 8-QAM constellations even without bandwidth compression. All results indicate the great potential of the proposed SRCD for SEFDM optical systems.

2. Principle

2.1. SEFDM system

Fig. 1 illustrates the basic principle of SEFDM. From the sketched spectra, we can see that the spacing between two neighboring sub-carriers in SEFDM is compressed by a BCF of α (< 1) compared to the conventional OFDM. Hence, the overall bandwidth can be further reduced by such an orthogonality violation. It should be noted that there are several existing algorithms for the generation of a real-valued SEFDM signal [26–33] in IM/DD optical communication systems. The modified fractional discrete Fourier transform (mFrDFT) proposed in [32] has great flexibility and compatibility, which is therefore used to generate SEFDM signals in this work. The generated real-valued SEFDM using mFrDFT can be expressed by

$$X = FS, \quad (1)$$

where S is an N -dimensional vector representing the symbols mapped in the frequency domain, X is an N -dimensional vector denoting the SEFDM symbol obtained in the time domain, and F is an $N \times N$ inverse mFrDFT (ImFrDFT) matrix. This matrix is given as:

$$F = \frac{1}{\sqrt{N}} \times \begin{bmatrix} e^{jk_1 n_1} & \dots & e^{jk_1 \left(\frac{N}{2} - N + n_2\right)} \\ \vdots & \ddots & \vdots \\ e^{jk_1 \left(\frac{N}{2} - N + k_2\right)} & \dots & e^{jk_1 (N - k_2)(N - n_2)} \end{bmatrix}, \quad (2)$$

where $\beta = j2\pi\alpha/N$. $k_1 = 0, 1, \dots, N/2 - 1$ and $k_2 = N/2 + 1, N/2 + 2, \dots, -N/2$ denote the row indices, $n_1 = 0, 1, \dots, N/2 - 1$ and $n_2 =$

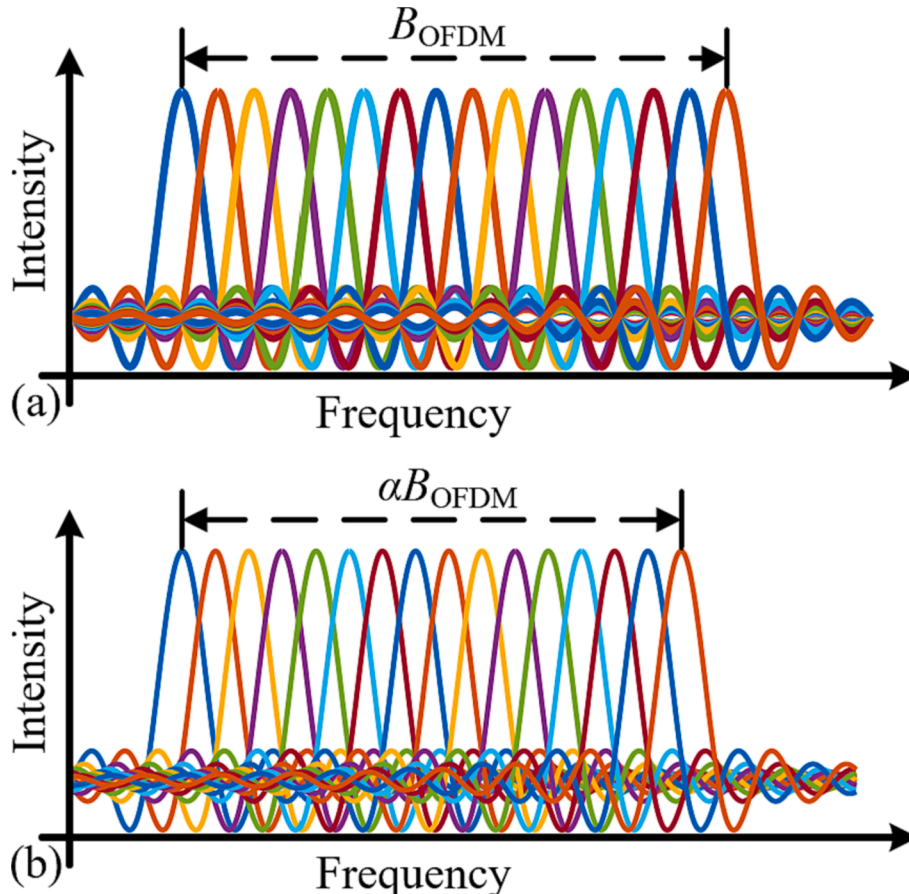


Fig. 1. The sketched spectra of (a) OFDM and (b) SEFDM ($\alpha = 0.9$).

$N/2 + 1, N/2 + 2, \dots, N-1$ represent the column indices. From (2), we can see that F can be divided into four submatrices separated by the $N/2$ -th row and the $N/2$ -th column. To generate a real-valued signal, we should ensure the symmetric property for the frequency distribution of the subcarriers. Thus, the elements of the $N/2$ -th row and the $N/2$ -th column are set as zero frequency, i.e. $e^{j\pi n_1}$, $e^{j\pi n_2}$, $e^{j\pi k_1}$, and $e^{j\pi k_2}$, respectively. It should be noted that F is the conventional IDFT matrix when $\alpha = 1$ and the system corresponds to OFDM, while it becomes SEFDM for $\alpha < 1$. The SE gain that SEFDM can achieve in comparison with OFDM is defined by [14]

$$\eta = \frac{1 - \alpha}{\alpha} \times 100\%. \quad (3)$$

Take $\alpha = 0.9$ as an example, SEFDM yields a spectral gain of 11.1 %.

In an additive white Gaussian noise (AWGN) channel, the received signal is given by

$$R = F^*(X + W) = CS + F^*W, \quad (4)$$

where the conjugate matrix F^* is the mFrDFT matrix and is used for demodulating the detected signal at the receiver side, $C = F^*F$ is the correlation matrix, and W represents the AWGN matrix. C is an identity matrix for $\alpha = 1$, while those off-diagonal elements of C are not zero for $\alpha < 1$, leading to self-created ICI.

2.2. SRCD

As aforementioned, additional decoding is necessary at the receiver side to remove the self-created ICI due to the non-zero off-diagonal elements of C . In the widely used ID algorithm [22], S can be reconstructed by the following iterative equation,

$$\hat{S}_l = R + (I - C)\hat{S}_{l-1}, \quad (5)$$

where \hat{S}_l is the estimated symbols after the l^{th} iterations, \hat{S}_{l-1} is the estimated symbols after the $(l-1)^{\text{th}}$ iterations, and I is an $N \times N$ identity matrix. The initial value \hat{S}_0 is set to R in this algorithm.

Each iteration consists of two steps, i.e., (1) iteration calculation and (2) the soft mapping applied to the estimated symbols after iteration calculation. For example, Fig. 2 depicts the soft mapping strategy of 4-QAM ID. The threshold interval is set to

$$\Delta d = 1 - \frac{l}{L}, \quad (6)$$

where L is the total number of iterations that we set in the ID

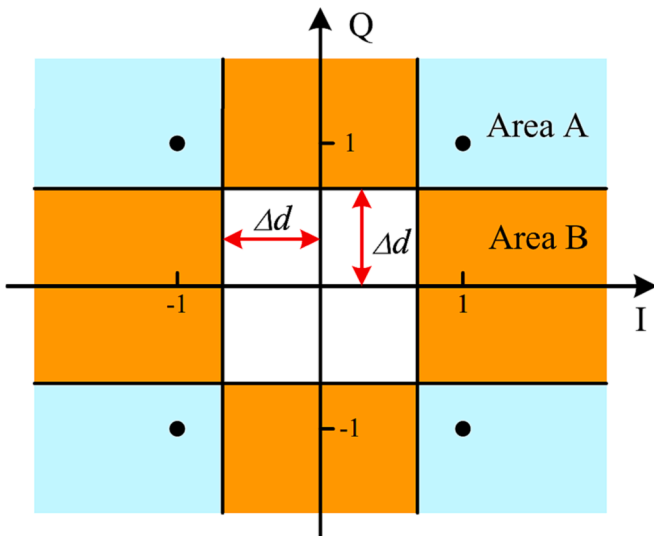


Fig. 2. Mapping strategy of 4-QAM ID.

algorithm. Only the symbols that fall in the threshold area (area A) are mapped onto the corresponding constellation points in each iteration, leaving the other symbols unchanged. By setting the threshold interval converging from near zero to the hard decision boundaries, we can make decisions on the calculated symbols with increasing confidence and less ICI interference.

Nonetheless, we can see that the performance of this 4-QAM ID is not optimal. During the mapping process, only the symbols located in area A satisfying both in-phase and quadrature threshold restrictions are mapped in each iteration. However, those symbols located in area B also have high confidence in one component (I or Q), but cannot be efficiently utilized in this case, leading to suboptimal decoding performance. Although the CBID algorithm proposed in [24] can solve this problem by I/Q separate mapping, it can only be used for squared QAM constellations due to its joint iteration of the I/Q components, which results in its relatively poor compatibility and flexibility. To solve this problem, the SRCD has therefore been proposed in this work.

Notice that the correlation matrix C is a real-valued matrix. Hence, in the proposed SRCD, the decoding process of in-phase and quadrature components in (5) can be calculated separately as

$$\begin{aligned} \text{real}(\hat{S}_l) &= \text{real}(R) + (I - C)\text{real}(\hat{S}_{l-1}) \\ \text{imag}(\hat{S}_l) &= \text{imag}(R) + (I - C)\text{imag}(\hat{S}_{l-1}), \end{aligned} \quad (7)$$

where $\text{real}(\cdot)$ and $\text{imag}(\cdot)$ denote the real part and the imaginary part of a complex number or vector, respectively. Eq. (7) shows that the real-valued property of the correlation matrix C can be utilized to separately decode the I/Q components of received complex-valued symbols, leading to increased compatibility and flexibility compared to the CBID algorithm.

We assume that the number of possible levels for one component (I or Q) is M . Then, the value of the level is chosen from $\{\pm 1, \pm 3, \dots, \pm(M-1)\}$, which can be seen as the sum of $(M-1)$ binary phase-shift keying (BPSK) signals. Similar to the concept of CBID proposed in [24], the ID process can be therefore broken into $(M-1)$ stages. Finally, this component of symbols can be decoded by $(M-1)$ stages of real-valued cascaded BPSK ID. The procedure of detection is illustrated in Fig. 3, where $M = 4$ in this example.

Let R_m be the output symbols of the $(m-1)^{\text{th}}$ stage as well as the input of the m^{th} stage, and S_m be the output symbols of the m^{th} stage. The relationship between R_m and S_m is given by

$$R_m = R_{m-1} - CS_{m-1}. \quad (8)$$

In the m^{th} stage, the iteration for I or Q components is the same as (7), except the threshold interval during the mapping process is changed as

$$\Delta d_m = (M - m)(1 - l/L). \quad (9)$$

The final output of one component is $\bar{S} = \sum_m S_m$. Hence, we can easily realize the demodulation of QAM symbols with rectangular constellations by using this scheme, which cannot be directly achieved by the conventional CBID.

3. Experimental setup

The experimental setup and the digital signal processing (DSP) are depicted in Fig. 4. The SEFDM signals were generated offline using MATLAB. The pseudo-random binary sequence (PRBS) was first generated and mapped onto 8-QAM symbols at the transmitter side. Then, $(N/2 - 1)$ effective subcarriers are mapped with 8-QAM symbols and used to perform Hermitian symmetry, along with an $N \times N$ ImFrDFT matrix, for the generation of a real-valued SEFDM signal, where N was set to 128. The zero-frequency subcarriers are reserved for the DC bias. After that, the cyclic prefix (CP) with a length of $1/16$ of one SEFDM symbol was added to combat CD. To estimate the channel response, 30 blocks of 4-QAM training sequences (TSs) were added before 530 blocks of SEFDM payload symbols. After parallel-to-serial (P/S) conversion, the

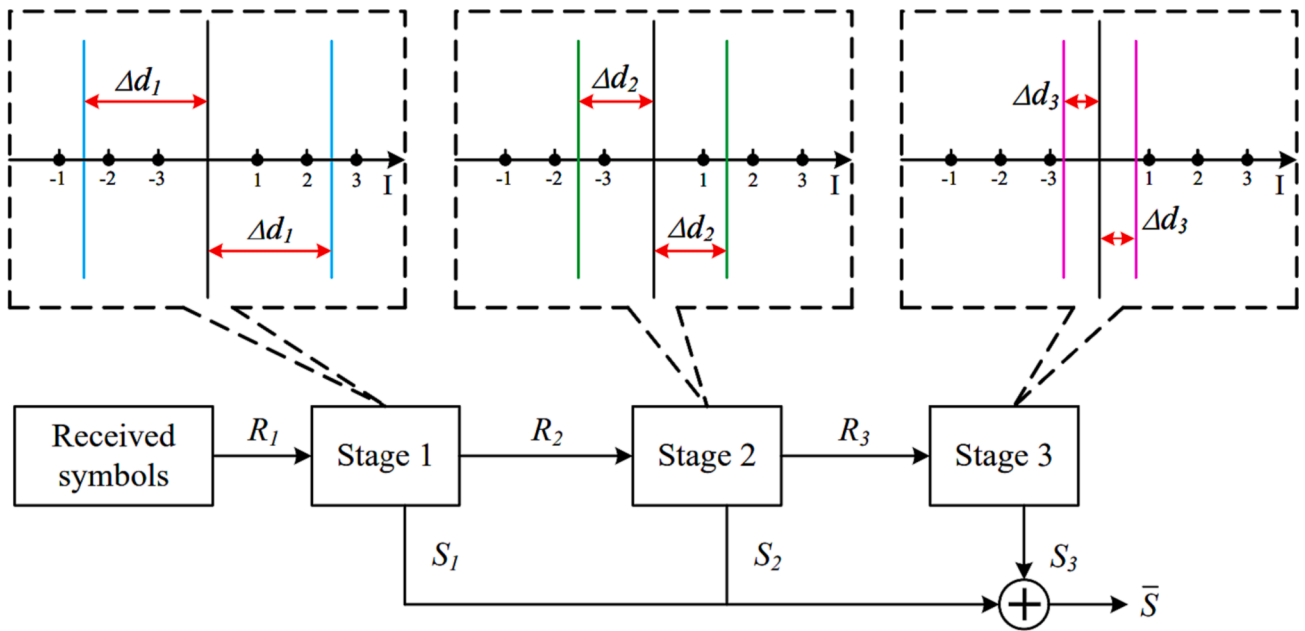


Fig. 3. Example cascaded BPSK iterative detecting structure for $M = 4$.

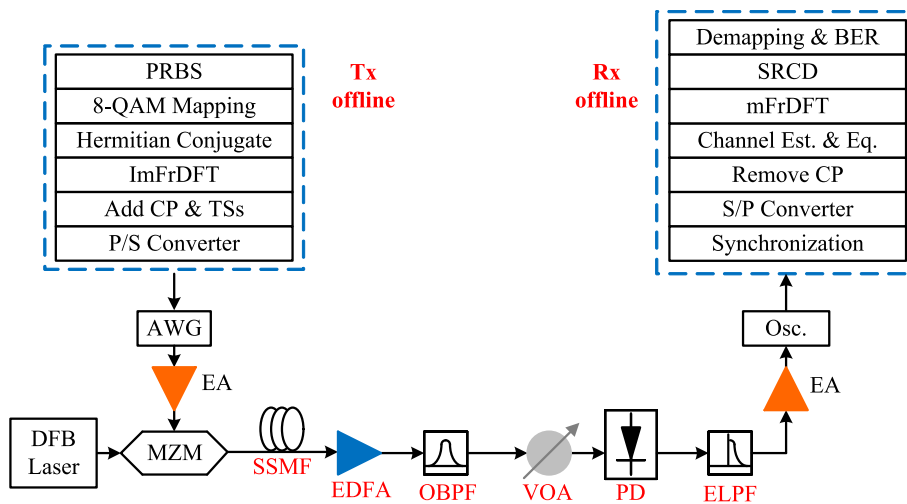


Fig. 4. Experimental setup and DSP for SEFDM transmission over SSMF (DFB Laser: distributed feedback laser, AWG: arbitrary waveform generator, EA: electrical amplifier, MZM: Mach-Zehnder modulator, SSMF: standard single mode fiber, EDFA: Erbium-doped fiber amplifier, OBPF: optical bandpass filter, VOA: variable optical attenuator, PD: photodiode, ELPF: electrical low pass filter).

generated real-valued digital signal was transformed into an analog signal by using a 12-GSa/s arbitrary waveform generator (AWG) (Tektronix 7122C). Therefore, the data rate of this 8-QAM SEFDM signal is $15.78(\approx 12 \times 3 \times 63/128 \times 16/17 \times 530/560)$ Gb/s. The output signal from AWG was first amplified by an electrical amplifier (EA, SHF 806E) with 26-dB gain. A narrow-linewidth tunable laser (NKT Koheras ADJUSTIK) with a central wavelength at 1550 nm and output optical power of 5-dBm was utilized as the laser source. Then, a Mach-Zehnder modulator (MZM) biased at the quadrature point converted the amplified electrical signal into the optical domain.

After 50-km standard single-mode fiber (SSMF) transmission, an erbium-doped fiber amplifier (EDFA, Amonics AEDFA-PA-30) was inserted as a preamplifier to compensate for the link loss, followed by an optical bandpass filter (OBPF, BVF-300CL) to remove the out-of-band amplified spontaneous emission (ASE) noise. Then, a variable optical attenuator (VOA) was employed to set the received optical power (ROP) for the performance evaluation. The signal was detected by a 50-GHz

photodiode (PD, XPDV 2020R) integrated with another EA (SHF 806E) with 26-dB gain. Before being captured by a real-time oscilloscope (KEYSIGHT DSAV334A) operating at 20-GSa/s, we used an electrical low pass filter (ELPF) with 7.2-GHz bandwidth to filter out the out-of-band noise. Fig. 6(a) and Fig. 6(b) show that the channel response of our system is relatively flat. In this work, we also used another ELPF with 5.5 GHz bandwidth to investigate the performance of our scheme working in a bandwidth-limited scenario, where its channel response is shown in Fig. 6(c) and Fig. 6(d). In the receiver side DSP, frame synchronization was performed before serial-to-parallel (S/P) conversion, CP removal, channel estimation and equalization [34]. The SEFDM demodulation was then implemented by the mFrDFT. To eliminate the purposely-induced ICI, either ID or the proposed SRCD was employed. The specially designed mapping strategies using the ID algorithm for these four 8-QAM formats are illustrated in Fig. 5, where the square 8-QAM depicted in Fig. 5(c) does not have the constellation point of (0, 0), so it is very different from those classical 'squared QAM' formats. To

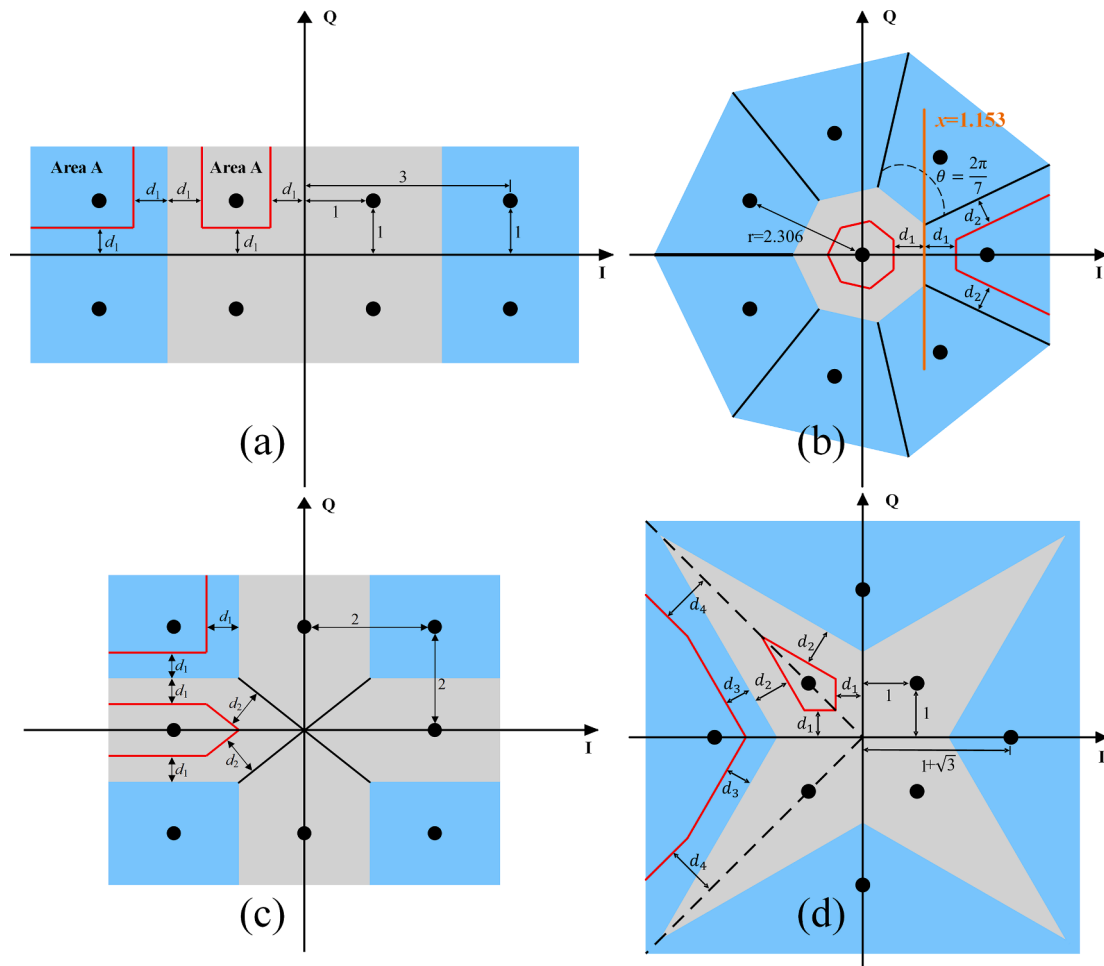


Fig. 5. Specially designed mapping strategies using the ID algorithm for (a) rectangular 8-QAM constellation, (b) circular 8-QAM constellation, (c) square 8-QAM constellation, and (d) star 8-QAM constellation.

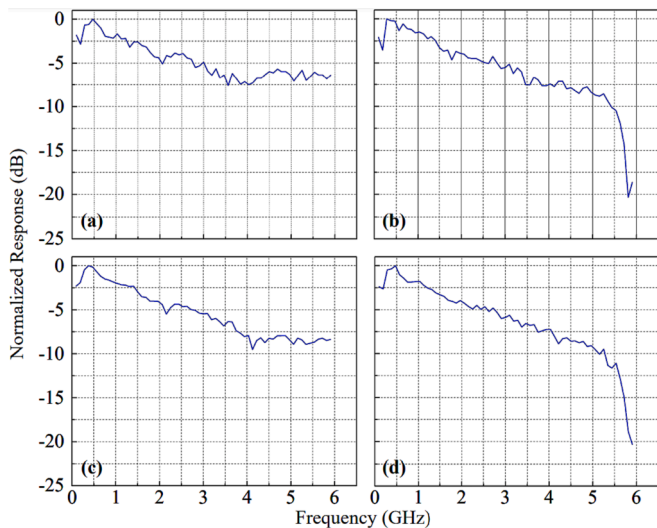


Fig. 6. Channel response with a 7.2-GHz ELPF at (a) BTB, (b) 50 km transmission, and with a 5.5-GHz ELPF at (c) BTB, (d) 50 km transmission.

illustrate the actual meaning of the distance labels ' $d_1 - d_4$ ' in Fig. 5, we can take Fig. 5(b) as an example. The hard decision boundary between the constellation points (0, 0) and (2.306, 0) is $x = 1.153$, and then the distance from these two points to the hard decision boundary is both

1.153. Thus, the update of d_1 is similar to Eq. (6), but needs to be multiplied by a coefficient of 1.153 based on the ID algorithm. It should be noted that SRCD can only be applied to the rectangular 8-QAM format among all four 8-QAM formats shown in Fig. 5. After ICI elimination and QAM de-mapping, the bit-error rate (BER) was finally calculated.

4. Experimental results

This section describes the back-to-back (BTB) and 50-km SSMF transmission performance of the SEFDM signals in the C-band. In Section 4.1, the ELPF used had a bandwidth of 7.2-GHz to emulate a system with a relatively flat channel response. Fig. 7 presents the electrical spectra of the received SEFDM signals with different α . In Section 4.2, the ELPF used had a bandwidth of 5.5 GHz to emulate a bandwidth-limited system.

4.1. Experimental results based on 7.2-GHz ELPF

Fig. 8 shows the transmission performance of the SEFDM signals with different BCFs and different 8-QAM formats after BTB and 50-km transmission, respectively, where the soft-decision (SD) forward error correction (FEC) threshold (2×10^{-2}), hard-decision (HD) FEC threshold (4.7×10^{-3}) [35], and KP4-FEC threshold (2.2×10^{-4}) are given for performance evaluation. The ID was applied to all 8-QAM formats, where the number of iterations has been optimized for different α . Meanwhile, the proposed SRCD was employed in the rectangular 8-QAM SEFDM system for comparison with the conventional ID

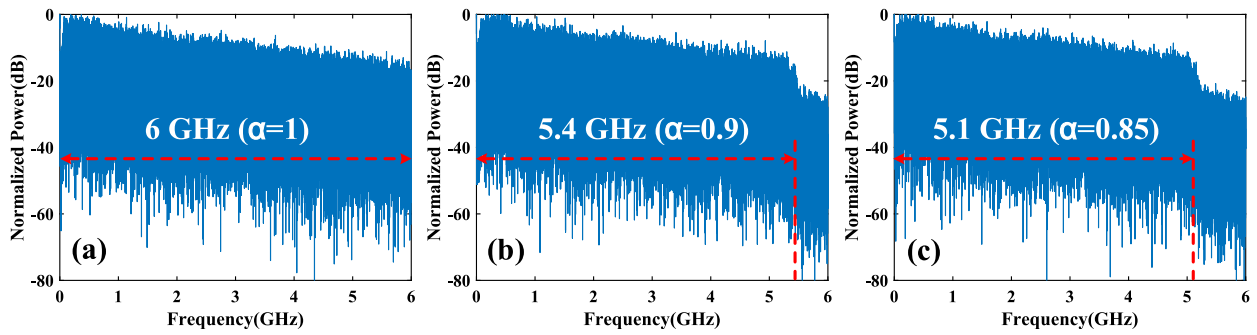


Fig. 7. The electrical spectra of the received SEFDM signals with a BCF of (a) 1, (b) 0.9, and (c) 0.85, respectively, where the bandwidth of the ELPF is 7.2 GHz.

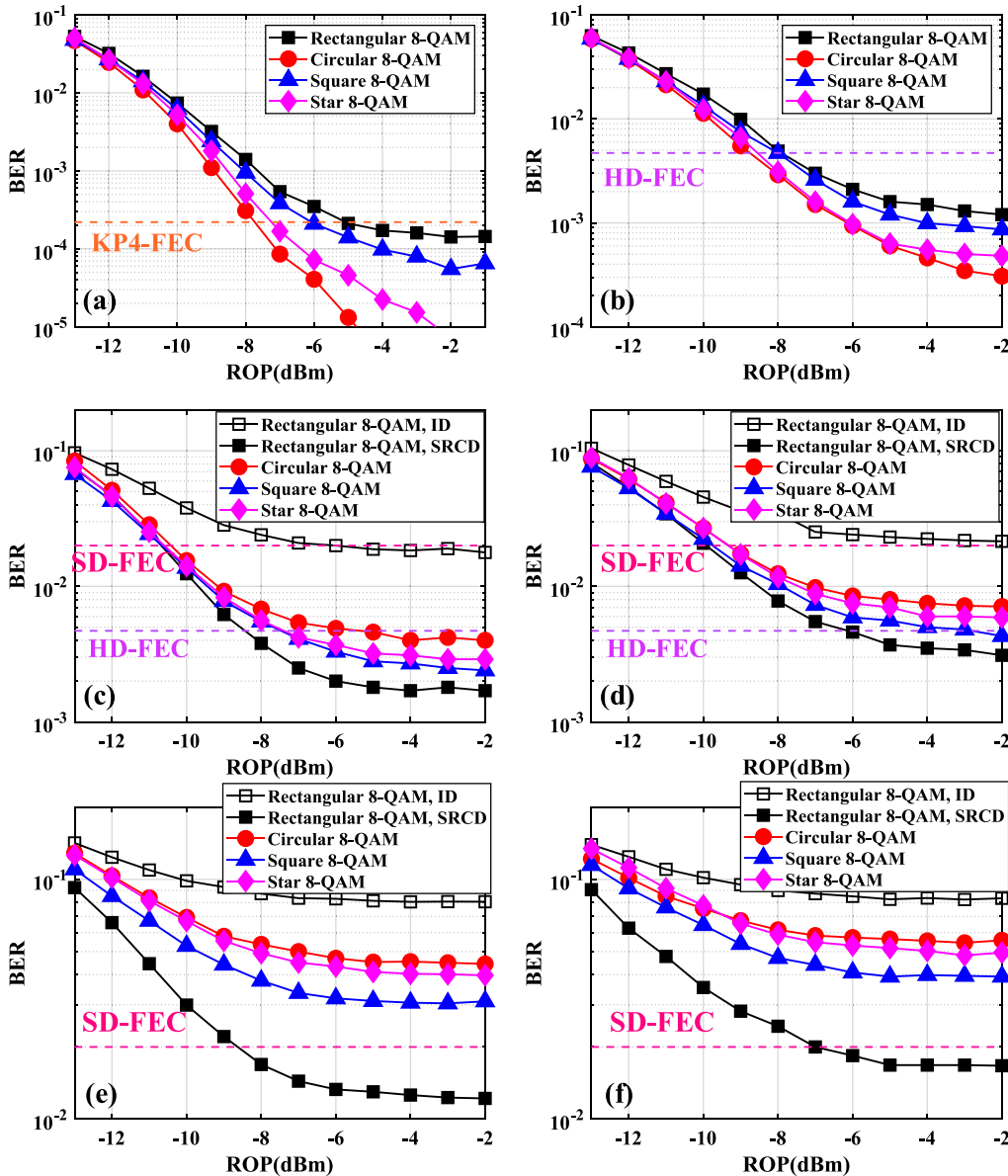


Fig. 8. Measured BER versus ROP at BTB with (a) $\alpha = 1$, (c) $\alpha = 0.9$, and (e) $\alpha = 0.85$, and after 50-km transmission with (b) $\alpha = 1$, (d) $\alpha = 0.9$, and (f) $\alpha = 0.85$, where the bandwidth of the ELPF is 7.2-GHz.

algorithm. For $\alpha < 1$, we can see from Fig. 8 that the SRCD outperforms the ID in the rectangular 8-QAM SEFDM system. Moreover, the performance gap between the two decoders increases with the decrease of α , indicating the superiority of the proposed SRCD. This can be attributed

to the I/Q separation during the decoding process in SRCD, guaranteeing more efficient ICI elimination. The received constellation diagrams of rectangular 8-QAM SEFDM signals with $\alpha = 0.9$ using ID and SRCD are compared in Fig. 9, verifying the effectiveness of the proposed SRCD.

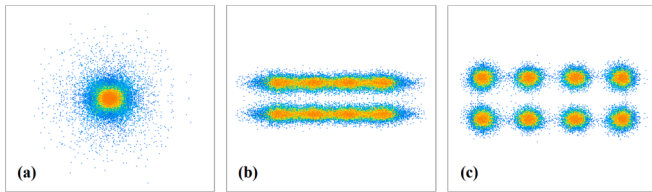


Fig. 9. Received constellations of the rectangular 8-QAM SEFDM signal with $\alpha = 0.9$ (a) before ICI elimination, (b) after ID, and (c) after SRCD.

Meanwhile, we can see from Fig. 8 that for different α , the optimal 8-QAM constellation is also different. For instance, when $\alpha = 1$ corresponding to the conventional OFDM system, the circular 8-QAM performs best due to its largest Euclidean distance [25], while the rectangular 8-QAM with SRCD performs best for $\alpha = 0.9$ and 0.85. This performance ranking under $\alpha = 0.9$ and 0.85 are caused by the sensitivity of the ID algorithm to different 8-QAM formats, which means that the ID algorithm is more effective for square 8-QAM format than the other three types of 8-QAM formats in eliminating the ICI. To verify our assumption, in Fig. 10, we give the BER performance of four 8-QAM formats using the log-MAP Viterbi decoder which is a maximum likelihood demodulation algorithm and is insensitive to different 8-QAM modulation formats, where the number of surviving paths for the log-MAP Viterbi decoder was set to 8 which can yield the saturate performance [14]. It can be seen from Fig. 10 that in the case of using the log-MAP Viterbi decoder, the performance ranking under $\alpha = 0.9$ and 0.85 with the log-MAP Viterbi decoder is the same as the conventional OFDM case shown in Fig. 8(a), verifying the above assumption.

4.2. Experimental results based on 5.5-GHz ELPF

We have also investigated the performance of the proposed scheme under a bandwidth-limited condition by replacing the 7.2-GHz ELPF with a 5.5-GHz ELPF. As shown in Fig. 11, we have studied BER versus BCF for different 8-QAM constellations. We can see from the figure that the rectangular 8-QAM can not provide a performance advantage with ID algorithm for $\alpha = 0.9$, and $\alpha = 0.85$ compared with $\alpha = 1$ since the ID algorithm has a limited ability in eliminating ICI. Meanwhile, the rectangular 8-QAM combined with the proposed SRCD achieves the optimal performance with a spectral gain of about 11.1 %, and becomes the only one meeting the HD-FEC requirement, indicating the effectiveness of the proposed scheme.

5. Summary

In this paper, we have proposed a novel soft-decision decoder, called SRCD, which presents improved compatibility and flexibility compared with the CBID algorithm, and achieve better performance compared with the conventional ID algorithm. The proposed scheme utilizes separate detection of the in-phase and the quadrature components of a complex-valued SEFDM signal based on the real-valued property of the correlation matrix, making it suitable for squared and rectangular QAM formats with more effective ICI elimination. Moreover, to the best of our knowledge, we first evaluated the performance of four types of 8-QAM formats employed in SEFDM systems. Experimental results show that the performance of ICI elimination for these four 8-QAM formats is also dependent on the decoder used at the receiver side. Finally, we have shown that when using the proposed SRCD, the SEFDM signal with the rectangular 8-QAM format corresponding to 11.1 % bandwidth compression can even outperform the OFDM signal modulated by all other 8-QAM formats in a bandwidth-limited optical system, indicating the great potential of the proposed scheme to be used in SEFDM optical systems.

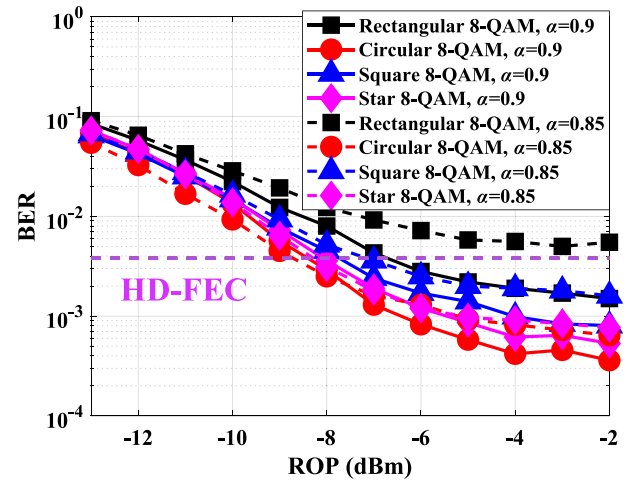


Fig. 10. Measured BER versus ROP after 50-km transmission with log-MAP Viterbi decoder, where the bandwidth of the ELPF is 7.2-GHz.

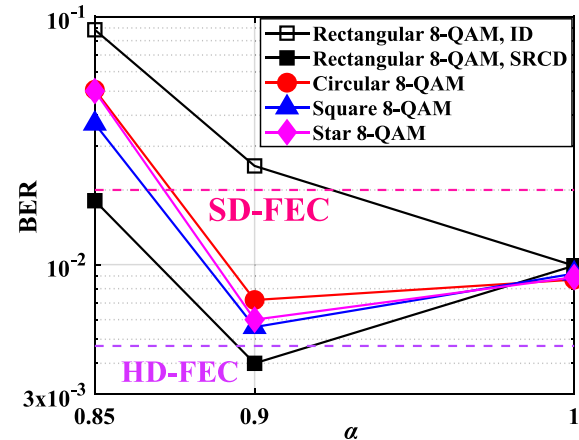


Fig. 11. Measured BER versus BCF after 50-km SSMF transmission at ROP = -2 dBm, where the bandwidth of the ELPF is 5.5-GHz.

CRedit authorship contribution statement

Peiji Song: Conceptualization, Methodology, Software, Validation, Formal analysis, Investigation, Data curation, Writing – original draft, Visualization. **Zhouyi Hu:** Supervision, Conceptualization, Methodology, Validation, Formal analysis, Writing – review & editing. **Hongyao Chen:** Writing – review & editing. **Chun-Kit Chan:** Supervision, Resources, Writing – review & editing, Project administration, Funding acquisition.

Declaration of Competing Interest

The authors declare that they have no known competing financial interests or personal relationships that could have appeared to influence the work reported in this paper.

Data availability

Data underlying the results presented in this paper are not publicly available at this time but may be obtained from the authors upon reasonable request.

Acknowledgement

This work was supported by Hong Kong Research Grants Council under Grant No. 14205820, and in part by the Interdisciplinary Research Project for Young Teachers of USTB (Fundamental Research Funds for the Central Universities) under Grant FRF-IDRY-21-019.

References

- [1] D. Qian, N. Cvijetic, J. Hu, T. Wang, 108 Gb/s OFDMA-PON with polarization multiplexing and direct detection, *J. Lightwave Technol.* 28 (4) (2010) 484–493.
- [2] F. Chang, S. Bhoja, New paradigm shift to PAM4 signaling at 100/400G for cloud data centers: a performance review, in: *Proc. Eur. Conf. Exhib. Opt. Commun., Gothenburg, Sweden, September 2017*, Paper W.1.A.5.
- [3] M.A. Khalighi, M. Uysal, Survey on free space optical communication: a communication theory perspective, *IEEE Commun. Surv. Tut.* 16 (4) (2014) 2231–2258.
- [4] E. Ip, A.P.T. Lau, D.J.F. Barros, J.M. Kahn, Coherent detection in optical fiber systems, *Opt. Express* 16 (2) (2008) 753–791.
- [5] R. Rodes, J. Estaran, B. Li, M. Muller, J. B. Jensen, T. Gruendl, M. Ortsiefer, C. Neumeyer, J. Rosskopf, K. J. Larsen, M.-C. Amann, I.T. Monroy, 100 Gb/s single VCSEL data transmission link, in: *Optical Fiber Communication Conference, Optical Society of America, March 2012*, paper PDP5D.10.
- [6] M.I. Olmedo, T. Zuo, J.B. Jensen, X.X. Qiwen Zhong, S. Popov, I.T. Monroy, Multiband carrierless amplitude phase modulation for high capacity optical data links, *J. Lightwave Technol.* 32 (4) (2013) 798–804.
- [7] J.C. Cartledge, A.S. Karar, 100 Gbit/s using intensity modulation and direct detection, in: *Proc. Eur. Conf. Exhib. Opt. Commun., London, UK, October 2013*, Paper We.4.C.3.
- [8] Y. Shao, R. Deng, J. He, K. Wu, L.K. Chen, Real-time 2.2-Gb/s water-air OFDM-OVC system with low-complexity transmitter-side DSP, *J. Lightwave Technol.* 38 (20) (2020) 5668–5675.
- [9] E. Bedeer, O.A. Dobre, M.H. Ahmed, K.E. Baddour, Joint optimization of bit and power loading for multicarrier systems, *IEEE Wirel. Commun. Lett.* 2 (4) (2013) 447–450.
- [10] I. Darwazeh, T. Xu, T. Gui, Y. Bao, Z. Li, Optical SEFDM system; bandwidth saving using non-orthogonal sub-carriers, *IEEE Photon. Technol. Lett.* 26 (4) (2013) 352–355.
- [11] Z. Li, F. Li, S. Qi, J. Li, J. Zhou, X. Yi, Z. Li, Beyond 100 Gb/s SEFDM signal IM/DD transmission utilizing TDE with 20 % bandwidth compression, *IEEE Commun. Lett.* 23 (11) (2019) 2017–2021.
- [12] J.E. Mazo, Faster-than-Nyquist signaling, *Bell Syst. Tech. J.* 54 (8) (1975) 1451–1462.
- [13] J. Zhou, Y. Qiao, T. Zhang, J. Wei, Q. Cheng, Q. Wang, Z. Yang, A. Zhang, Y. Lu, Faster than Nyquist non-orthogonal frequency division multiplexing for visible light communications, *IEEE Access* 6 (2018) 17933–17941.
- [14] B. Yu, C. Guo, L. Yi, H. Zhang, J. Liu, X. Dai, A.P.T. Lau, C. Lu, 150-Gb/s SEFDM IM/DD transmission using log-MAP Viterbi decoding for short reach optical links, *Opt. Express* 26 (24) (2018) 31075–31084.
- [15] Y. Jiang, W. Hager, J. Li, Tunable channel decomposition for MIMO communications using channel state information, *IEEE Trans. Signal Process.* 54 (11) (2006) 4405–4418.
- [16] B. Yu, L. Yi, C. Guo, J. Liu, X. Dai, A. Lau, C. Lu, Dispersion tolerant 66.7-Gb/s SEFDM IM/DD transmission over 77-km SSMF, in: *Proc. Eur. Conf. Exhib. Opt. Commun., Roma, Italy, September 2018*, pp. 1–3.
- [17] I. Kanaras, A. Chorti, M.R. Rodrigues, I. Darwazeh, Spectrally efficient FDM signals: bandwidth gain at the expense of receiver complexity, in *ICC'09. IEEE International Conference on Communications, 2009*, IEEE, 2009, pp. 1–6.
- [18] B. Muquet, Z. Wang, G. Giannakis, M. de Courville, P. Duhamel, Cyclic pre-fixing or zero padding for wireless multicarrier transmissions, *IEEE Trans. on Commun.* 50 (12) (2002) 2136–2148.
- [19] Y. Ding, T.N. Davidson, Z.Q. Luo, K.M. Wong, Minimum ber block pre-coders for zero-forcing equalization, *IEEE Trans. Signal Process.* 51 (9) (2003) 2410–2423.
- [20] J. Wang, J. Song, Z.X. Yang, L. Yang, J. Wang, Frames theoretic analysis of zero-padding ofdm over deep fading wireless channels, *IEEE Trans. Broadcast* 52 (2) (2006) 252–260.
- [21] T. Gui, K. Zhong, X. Zhou, L. Zhou, A. Lau, C. Lu, C. Nan, Efficient MMSE-SQRD-based MIMO decoder for SEFDM-based 2.4-Gb/s-spectrum-compressed WDM VLC system, *IEEE Photonics J.* 8 (4) (2016), 7905709.
- [22] S. Heydari, M. Ferdosizadeh, F. Marvasti, Iterative detection with soft decision in spectrally efficient FDM systems, *Tech. Rep. arXiv, 1304.4003v1*, 2013.
- [23] T. Xu, I. Darwazeh, M-QAM signal detection for a non-orthogonal system using an improved fixed sphere decoder, in: *Proc. 9th IEEE/IET Int. Symp. Commun. Syst., Netw. Digit. Sign, Manchester, U.K., July 2014*, pp. 623–627.
- [24] J. Huang, Q. Sui, Z. Li, F. Ji, Experimental demonstration of 16-QAM DD-SEFDM with cascaded BPSK iterative detection, *IEEE Photon. J.* 8 (3) (2016) 1–9.
- [25] P. Song, Z. Hu, C.K. Chan, Performance comparison of different 8-QAM constellations used in SEFDM systems, in: *Proc. Opto-Electronics and Communications Conference, Hong Kong, China, July 2021*, Paper T1B-4.
- [26] Y. Wang, Y. Zhou, T. Gui, K. Zhong, X. Zhou, L. Wang, A.P.T. Lau, C. Lu, N. Chi, SEFDM based spectrum compressed VLC system using RLS time-domain channel estimation and ID-FSD hybrid decoder, in: *Proc. Eur. Conf. Exhib. Opt. Commun., Düsseldorf, Germany, September 2016*, pp. 827–829.
- [27] T. Xu, S. Mikroulis, J.E. Mitchell, I. Darwazeh, Bandwidth compressed waveform for 60-GHz millimeter-wave radio over fiber experiment, *J. Lightwave Technol.* 34 (14) (2016) 3458–3465.
- [28] P. Whatmough, M. Perrett, S. Isam, I. Darwazeh, VLSI architecture for a reconfigurable spectrally efficient FDM baseband transmitter, *IEEE Trans. Circuits Syst. I.* 59 (5) (2012) 1107–1118.
- [29] C. Guo, B. Yu, L. Yi, J. Zhang, Y. Xu, X. Wu, J. Liu, H. Zhang, 98.7-Gb/s Optical SE-DMT transmission using an enhanced decision-directed algorithm with preconditions, in: *Proc. Asia Communications and Photonics Conference, Guangzhou, China, October 2017*, Paper S4B-2.
- [30] J. Zhou, Y. Qiao, Z. Yang, E. Sun, Faster-than-Nyquist non-orthogonal frequency-division multiplexing based on fractional Hartley transform, *Opt. Lett.* 41 (19) (2016) 4488–4491.
- [31] J. Zhou, Y. Qiao, Z. Yang, Q. Cheng, Q. Wang, M. Guo, X. Tang, Capacity limit for faster-than-Nyquist non-orthogonal frequency-division multiplexing signaling, *Sci. Rep.* 7 (2017) 3380.
- [32] Z. Hu, C.K. Chan, A modified fractional DFT based FTN-NOFDM technique for IM/DD optical systems, in: *Proc. Opto-Electronics and Communications Conference, Seogwipo City, South Korea, July 2018*, Paper 3B1-4.
- [33] Z. Hu, C.K. Chan, A novel baseband faster-than-Nyquist non-orthogonal FDM IM/DD system with block segmented soft-decision decoder, *J. Lightwave Technol.* 38 (3) (2019) 632–641.
- [34] Z. Hu, S. Gao, Y. Shao, L.K. Chen, C.K. Chan, A robust channel processor for faster-than-Nyquist non-orthogonal FDM visible light communication systems, in: *Proc. Eur. Conf. Exhib. Opt. Commun., Roma, Italy, September 2018*, pp. 1–3.
- [35] L. Zhang, F. Kschischang, Staircase codes with 6 % to 33 % overhead, *J. Lightwave Technol.* 32 (10) (2014) 1999–2002.